

Can Protostellar Jets Drive Supersonic Turbulence in Molecular Clouds?

Robi Banerjee¹, Ralf S. Klessen¹, Christian Fendt²

¹*Institute of Theoretical Astrophysics, University of Heidelberg, Albert-Ueberle-Str. 2, 69120 Heidelberg, Germany*

²*Max Planck Institute for Astronomy, Königsstuhl 17, 69117 Heidelberg*

ABSTRACT

Jets and outflows from young stellar objects are proposed candidates to drive supersonic turbulence in molecular clouds. Here, we present the results from multi-dimensional jet simulations where we investigate in detail the energy and momentum deposition from jets into their surrounding environment and quantify the character of the excited turbulence with velocity probability density functions. Our study includes jet-clump interaction, transient jets, and magnetised jets. We find that collimated supersonic jets do not excite supersonic motions far from the vicinity of the jet. Supersonic fluctuations are damped quickly and do not spread into the parent cloud. Instead subsonic, non-compressional modes occupy most of the excited volume. This is a generic feature which can not be fully circumvented by overdense jets or magnetic fields. Nevertheless, jets are able to leave strong imprints in their cloud structure and can disrupt dense clumps. Our results question the ability of collimated jets to sustain supersonic turbulence in molecular clouds.

Subject headings: magneto-hydrodynamics, ISM: evolution, methods: numerical

1. Introduction

The interstellar medium (ISM) and star forming molecular clouds are permeated by turbulent, supersonic gas motions (e.g. see recent reviews Elmegreen & Scalo 2004; Mac Low & Klessen 2004; Ballesteros-Paredes et al. 2007, and references therein). Supersonic turbulence is a main ingredient in the process of star formation. It can, on the one hand, compress material that might become Jeans unstable and collapse to form stars. On the other hand, supersonic motions can disperse clumps and cores in radiative shocks. Although supersonic turbulence is a major player in forming stars, its origin is still obscure. A difficulty of supersonic turbulence is that it decays quickly and has to be continuously driven to be maintained (Mac Low et al. 1998; Stone et al. 1998; Padoan et al. 1999). The energy input can in principle be provided by sources within the molecular cloud (e.g. radiation from massive stars, outflows) or from outside (e.g. supernovae, galactic spiral arms). In particular, the birth of stars is in most cases accompanied by outflows and high velocity jets. Protostellar jets propagate with velocities of about 300 km s^{-1} as seen in the radial velocity shift

of forbidden emission lines and proper motions of jet knots. Many of these jets remain highly collimated with opening angles less than 5° over a distance up to several pc (Mundt et al. 1990; Raga et al. 2001). As proposed first by Norman & Silk (1980), these Herbig-Haro (HH) outflows could sustain the energetics in molecular clouds. This is an attractive idea as this process could be self-regulated. The amount of turbulent energy controls the strength of gravitational collapse and subsequent star formation activity: an increased energy input from protostellar outflows results in higher levels of turbulence, which reduces the star formation activity. This in turn lowers the energy injection by outflows, increasing again the star formation rate.

In order to study the effects of jet-driven turbulence, it is useful to estimate the kinetic energy associated with protostellar jets, and compare it to the energy needed to drive supersonic turbulence in a typical star forming region. It should be mentioned that the simple analysis of the energies involved can at best be an order-of-magnitude approach. Real values may easily differ by factors of a few. However, it demonstrates that protostellar jets and outflows may indeed play an important role in determining density and velocity structure in star forming regions (see, e.g., Stanke 2000; Stanke et al. 2002).

We begin with an estimate of the protostellar jet kinetic luminosity. It can be described as

$$L_{\text{jet}} = \frac{1}{2} \dot{M}_{\text{jet}} v_{\text{jet}}^2 \approx 2.9 \times 10^{32} \text{ erg s}^{-1} \left(\frac{\dot{M}_{\text{jet}}}{10^{-8} \text{ M}_\odot \text{ yr}^{-1}} \right) \left(\frac{v_{\text{jet}}}{300 \text{ km s}^{-1}} \right)^2, \quad (1)$$

with $\dot{M}_{\text{jet}} \approx 10^{-8} \text{ M}_\odot \text{ yr}^{-1}$ being the mass loss associated with the jet material that departs from the protostellar disk system at typical velocities of $v_{\text{jet}} \approx 300 \text{ km s}^{-1}$. A simple estimate of the jet lifetime in this phase is $\tau_{\text{jet}} \approx (3 \text{ pc}/300 \text{ km s}^{-1}) \approx 10^4 \text{ yr}$ where we take a spatial extent of 3 pc. This coincides to within factors of a few with the typical duration of the class 0 and early class I phases of protostellar evolution. In these phases we expect the strongest outflow activity (see the review by Andre et al. 2000). This kinetic luminosity is less than but comparable to the radiative luminosity of protostars. The outflow-ISM coupling is more direct and, thus, supposedly more efficient than the energy exchange between the protostellar radiation and the ISM. However, the detailed coupling strength is not known and will be investigated here. The total amount of energy provided by the jet is

$$E_{\text{jet}} = L_{\text{jet}} \tau_{\text{jet}} \approx 10^{44} \text{ erg}. \quad (2)$$

If we assume a typical cluster-forming region of molecular cloud material, say with mass $M = 1000 \text{ M}_\odot = 2 \times 10^{36} \text{ g}$ and a rms velocity dispersion of $v_{\text{rms}} = 1 \text{ km s}^{-1}$ (corresponding to a Mach 5 flow at the canonical cloud temperature of 10 K), then the total turbulent kinetic energy in the region is

$$E_{\text{kin}} = \frac{1}{2} M v_{\text{rms}}^2 \approx 10^{46} \text{ erg}. \quad (3)$$

In principle, this means that

$$N_{\text{jet}} = f E_{\text{kin}}/E_{\text{jet}} \approx 100 f, \quad (4)$$

jets could carry enough energy to drive the turbulence if the coupling to the ambient medium, f , is reasonable efficient. Given that a molecular cloud region of $M = 1000 M_{\odot}$ will form a cluster of several thousand stars (see e.g., the Orion Nebula cluster, Hillenbrand 1997) protostellar jets are serious candidates to drive turbulence in star-forming regions.

This analysis, however, is incomplete without a comparison of timescales. We have estimated the lifetime of individual jets being of order of 10^4 years. This has to be compared with the decay timescale of turbulence in the star-forming region. The dissipation of supersonic turbulence is roughly

$$\dot{E}_{\text{kin}} = -\eta M k v_{\text{rms}}^3, \quad (5)$$

with $\eta \approx 0.07$ (Mac Low 1999). M is the total mass, k the wavenumber of the most dominant velocity mode, and again v_{rms} the rms velocity dispersion. We know from observations (e.g., Ossenkopf & Mac Low 2002) that molecular cloud turbulence always is dominated by the largest-scale modes, we thus take $k = 1/L$ with $L \approx 1$ pc being the size of the star-forming region. The timescale for turbulent decay then becomes

$$\tau_{\text{decay}} = E_{\text{kin}}/\dot{E}_{\text{kin}} = \frac{1}{2\eta} \frac{L}{v_{\text{rms}}} \approx 6.8 \times 10^6 \text{ yr} \left(\frac{L}{1 \text{ pc}} \right) \left(\frac{v_{\text{rms}}}{1 \text{ km s}^{-1}} \right)^{-1}. \quad (6)$$

Turbulence decays on several rms crossing times L/v_{rms} , which is considerably larger than the lifetime of individual jets. The energy inserted by individual jets and outflows therefore will remain in the cloud region during most of its star-formation period, which typically lasts a few 10^5 years (Klessen 2003; Mac Low & Klessen 2004). This simple estimate indicates that protostellar jets and outflows indeed carry sufficient energy to drive turbulence. The question that remains, is whether this energy can be transferred to the ambient cloud material with high-enough efficiency and with the right spatial and temporal characteristics.

Recently, the idea of jet-driven turbulence has been reconsidered in phenomenological estimates (Matzner 2007; Quillen et al. 2005) and several numerical simulations (e.g., Chernin et al. 1994; de Gouveia Dal Pino 1999; Mac Low 2000; Micono et al. 2000; Li & Nakamura 2006; Cunningham et al. 2006a,b). In particular, direct numerical simulations of this issue have the possibility to answer the question whether outflows and jets can drive supersonic turbulence in molecular clouds. One of the first numerical study of outflow driven turbulence was done by Mac Low (2000). This work showed (with randomly placed spherical and collimated outflow sources in a molecular cloud) that the excited turbulence decays quickly and that such point source driven turbulence is highly dissipative. A more recent numerical investigation with the same resolution was done by Li & Nakamura (2006). There the outflow sources were launched in regions where protostars formed. Therefore, back-reactions from multiple outflows in star forming regions could be studied self-consistently. These authors claim that the outflows generated by their protostellar objects maintain the turbulence in the molecular cloud, although it is difficult to distinguish between the driving forces – gravity or outflows – from their simulation.

Detailed numerical studies of isolated jets by Chernin et al. (1994) showed that low Mach

number jets entrain gas along their edges via Kelvin-Helmholtz instabilities and high Mach number jets transfer energy and momentum mainly through the bow shock region at the head of the jets. A similar study but for supersonic jets showed that a large fraction of the jet momentum can be transferred to the ambient medium (Micono et al. 2000). However, this investigation concentrated on global properties of the energy and momentum transfer but did not quantify the amount and structure of the excited turbulence. Numerical investigations by Cunningham et al. (2006a) showed that momentum entrainment of the surrounding gas actually is reduced in jet-jet interactions. The redirected radiative jets are not spread out widely in this process, limiting the ability to strongly impact the jet environment. On the other hand, Cunningham et al. (2006b) found that cavities produced by decaying jets stir up the gas inside the cavities while they are back-filled. The idea of cavity driven turbulence was recently put forward by Quillen et al. (2005) who compared the energetics of expanding cavities by wind blown bubbles and outflows NCG 1333 with the energy necessary to power turbulence in this molecular cloud. The authors conclude that the energy from outflows seen in ^{12}CO and the observed cavities is sufficient to maintain turbulence in the nebula (see also Warin et al. 1996; Knee & Sandell 2000, for outflow activities in NGC1333).

Another important aspect of jet entrainment, namely the influence of radiative cooling, was recently presented by Moraghan et al. (2006). For high velocity jets it is the Mach number that determines the shape and size of the jet and its bow shock, whereas for lower velocity jets the cooling efficiency plays a crucial role in shaping the jet entrained environment. If the gas can cool efficiently, lower velocity jets stay more collimated and are less likely to develop large instabilities compared the non-radiative jets. Here, we are mainly interested in high velocity jets as a potential source of supersonic turbulence. For those, radiative effects are of minor influence. We therefore use an isothermal equation of state (EOS) throughout the presented study.

We note there is a literature concerning the question of possible jet-driven molecular outflows, in particular to explain the mass-velocity relation (usually a power law $dm(v)/dv \sim (v/v_{\text{jet}})^{-\alpha}$) and/or the outflow velocity-distance relation (a linear "Hubble law" increase with distance) observed in molecular outflows (e.g. Stahler 1994; Lada & Fich 1996). Numerical simulations which try to explain these findings, however, concentrate on the momentum exchange from jets to ambient medium and do not investigate the turbulence pattern induced by this interaction (see e.g. Downes & Ray 1999; O'Sullivan & Ray 2000; Downes & Cabrit 2003; Rosen & Smith 2004).

Jets can travel over a long distance and are likely to interact with density lumps on their way. One of the first numerical studies of jet–cloud core interaction was carried out by Raga & Canto (1995). This work showed that jets are highly deflected and de-collimated if the density contrast between the jet and the dense clump is very high. Whether jets can penetrate cloud cores and disrupt them, or are just deflected, will have an impact on the cloud structure. To address this point we present one example of jet–clump interaction in this work.

If jets are the main driver of supersonic turbulence in molecular clouds they have to impart high velocities to a large fraction of the cloud material with high velocities. On the one hand, such

jets have large momenta, but on the other hand, highly supersonic jets are well collimated and do not entrain much gas. These general jet properties are also seen in the SPH simulations by Chernin et al. (1994). In Cunningham et al. (2006a) the authors concluded that the most efficient coupling of outflows with their surrounding cloud will be by low-velocity fossil outflows. But, such low-velocity jets are unlikely sources of *supersonic* turbulence.

In this study we present the results from numerical simulations of individual jets interacting with their surrounding gas. We focus on the impact of collimated jets on their environment, in particular, on the jet-excited velocity structure in the surrounding gas. To quantify the impact of jets on the cloud we present velocity probability density functions (PDFs) for a number of different setups. These include two and three dimensional jets, transient jets (jets whose powering engines are shut off during the simulation), jet–clump interactions, and jets that run into a magnetised environment. The presented probability density functions can be interpreted as volume filling factors of fluctuations with certain amplitudes. These diagrams show that the fraction of fluctuations excited by jets that reach supersonic velocities is negligibly small. Additionally, any supersonic excitations do not propagate far into the cloud and decay rapidly.

2. Numerical Method

We performed the numerical investigation with the adaptive mesh refinement (AMR) code FLASH (Fryxell et al. 2000) in which we model the jet as a kinetic energy injection from the box boundary. We parametrise the jet speed by its Mach number, \mathcal{M} . In our simulations, the temperature of the jet medium and ambient medium are the same, which means that the internal and external jet Mach numbers are equal. For most of our simulations the density of the jet material, ρ_{jet} , and the ambient medium, ρ_{amb} , are also equal but the jet density can be varied with the contrast parameter $\delta = \rho_{\text{jet}}/\rho_{\text{amb}}$. The energy injection can be switched on and off after a certain amount of time. We denote a jet that is not continuously driven a transient jet. Typically our jet runs into a homogeneous density distribution, but we also present a study of jet–clump interaction where the jet runs into a spherical over-density, ρ_{cl} , with a density contrast given by $\delta_{\text{cl}} = \rho_{\text{cl}}/\rho_{\text{amb}}$. Furthermore, we present studies where the jet runs into a magnetised medium where the homogeneous magnetic field is either parallel or perpendicular to the jet axis. In all cases we use the ideal HD and MHD treatment of the FLASH code and neglect physical viscous and resistive effects. For the MHD runs we use the standard diffusive cleaning of magnetic field divergence. In Table 1 we summarise the parameters for our different simulation runs.

We use outflow boundary conditions on the non-injection side of the simulation box and constant boundary conditions on the side where the wind is injected. For all but one simulations we use an isothermal equation of state approximated by an adiabatic index of $\gamma = 1.0001$. Note that the FLASH code always evolves the entire energy (i.e. kinetic, magnetic and thermal energy) within its standard advection scheme and does not include a treatment for a pure isothermal gas. For comparison we also show the results of one barotropic run (i.e. $p \propto \rho^\gamma$) with a barotropic index of

$\gamma = 1.4$.

As we do not include radiative processes in our simulations (for simplicity and to limit the parameter space) we present our results in simulation units and give some examples to convert them to physical units. We choose units where the density of the ambient medium is unity ($\rho_{\text{amb}} = 1$) and so is the pressure. Therefore, the sound speed is unity throughout the simulation ($c_s = 1$) and the unit of the gas velocity corresponds also to the sonic Mach number. For example if we assume a mean number density of 10^3 cm^{-3} , a mean molecular weight of $\mu = 2.1$ (i.e. $\rho = 3.51 \times 10^{-21} \text{ g cm}^{-3}$), and a gas temperature of $T = 10 \text{ K}$ (i.e. $c_s = 0.198 \text{ km s}^{-1}$) a Mach 5 jet has a flow speed of $\sim 1 \text{ km s}^{-1}$. If we furthermore choose the length of the simulation box to be 1 pc ($L_{\text{Box}} = 24 \text{ length units}$; 1 length unit = $1.286 \times 10^{17} \text{ cm}$), one time unit corresponds to 2.05×10^5 years.

Our simulation boxes have dimensions of 24×8 and $24 \times 8 \times 8$ length units in the 2D and 3D cases. Note that the images presented show only subareas of the full simulation box.

The initial grid is resolved with up to 5 refinement levels which corresponds to an effective resolution of 128 grid points in the y -direction (and z -direction in the 3D cases) and 3×128 grid points in the x -direction. Furthermore we allow for maximal 8 refinement levels (7 in the 3D cases) during runtime. We use the standard second-derivative refinement criterion based on the gas density. This refinement criterion is particular useful to capture density contrasts which allows us to track propagating shock fronts at high resolution. The effective resolution corresponding to 8 refinement levels is 1024 grid points in the y -direction and 3×1024 along the jet axis (x -direction).

3. Analysis and Results

Our main focus is the question whether jets from young stellar objects can excite *supersonic* turbulent motions in their parent cloud. For this purpose we inject jets with different properties into an ambient medium that is either homogeneous or clumpy. A well known general trend is that high velocity flows ($\mathcal{M} \gg 1$) generate less pronounced instabilities. For instance, Kelvin-Helmholtz instabilities at the edge of the jet will appear only at very large wavenumbers, i.e. small wavelengths, which will decay quickly. The width of the bow shock also shrinks with increasing jet speed. Furthermore, fast jets are less prone to deflections on clumps and are only slightly redirected in jet-jet interactions (Cunningham et al. 2006a). The most distinctive impact on the environment by means of efficient gas entrainment comes from flows that are transonic or only mildly supersonic. Transient jets naturally reach such a transonic state. 'Dying' jets leave fossil cavities that couple quite well to the molecular cloud (Cunningham et al. 2006b). We discuss the effects of such transient jets in this section.

To study the impact of jets on their surrounding media it is quite useful to quantify explicitly the jet-excited motions of the gas. A good way of doing this is to calculate the relative strength of particular velocity excitations and follow their time evolution. For this purpose we quantify the strength of the (turbulent) fluctuations produced by the jet with probability density function

(PDF) for velocity fluctuations, v

$$P(f_i) = \sum_j w_j(f_i) \quad (7)$$

$$w_j(f_i) = \{\Delta V_j / \mathcal{V} \mid f_i \leq f_j < f_{i+1}\}, \quad (8)$$

where $\Delta V_j / \mathcal{V}$ is the relative volume occupied by the quantity f_j at the mesh point j , and $[f_i, f_{i+1}]$ is the bin range for the i 'th bin in which f_j is sampled. With this definition the PDF is normalised, i.e.

$$\sum_i P_i = 1, \quad (9)$$

so the P_i 's can be interpreted as volume filling factors of a particular velocity interval. For the calculation of the presented PDFs we only take into account the volume \mathcal{V} which is affected by the jet at each time, i.e.

$$\mathcal{V} = \sum_i V_i \quad \text{with} \quad \{i \mid v_i \neq 0\} \quad (10)$$

which is the volume with non-zero velocity fluctuations v_i . With the help of the above described PDFs one can accurately measure the fraction of sub- and supersonic gas motions.

The quantification of turbulent structure with the help of density or velocity PDFs is often used in numerical simulations (e.g. Vazquez-Semadeni 1994; Chernin et al. 1994; Falgarone et al. 1994; Lis et al. 1996; Klessen 2000; Li et al. 2003; Mac Low et al. 2005; Padoan et al. 2007). For supersonic turbulence the generated density fluctuations can often be fitted by a log-normal distribution which width is mainly determined by the *rms* Mach number of the flow and similar holds for the velocity PDF. Here we use velocity PDFs (or volume weighted histograms) to distinguish between sub- and supersonic fluctuations. For all of presented cases this distinction comes about naturally: the supersonic regime is strongly suppressed compared to the subsonic regime. We also tried to fit log-normal distribution to the PDFs in the subsonic regime, but their application are of limited use because of the complex structure in velocity space (e.g. double or multiple peaks).

Furthermore, we compute contributions to the kinetic energy from the subsonic and supersonic regimes separately and show their time evolution. From these calculations one can derive decay laws for the two different regimes and compare their importance to the overall energy with time.

3.1. General Jet Properties, Continuous vs. Transient jets

We begin our investigation with the results from two dimensional (slab) jets that are either continuously driven or have energy injection shut off after a time $t = 1.3$. In Fig. 1 we show the time evolution of the density and velocity of our fiducial run: a Mach 5 jet running into a homogeneous medium. Further parameters of this run are: no density contrast ($\delta = 1$) and no magnetic fields. The jet is continuously powered. This medium Mach number jet develops knots inside the jet and visible Kelvin-Helmholtz instabilities, including 'cats-eyes', at the edge of the jet.

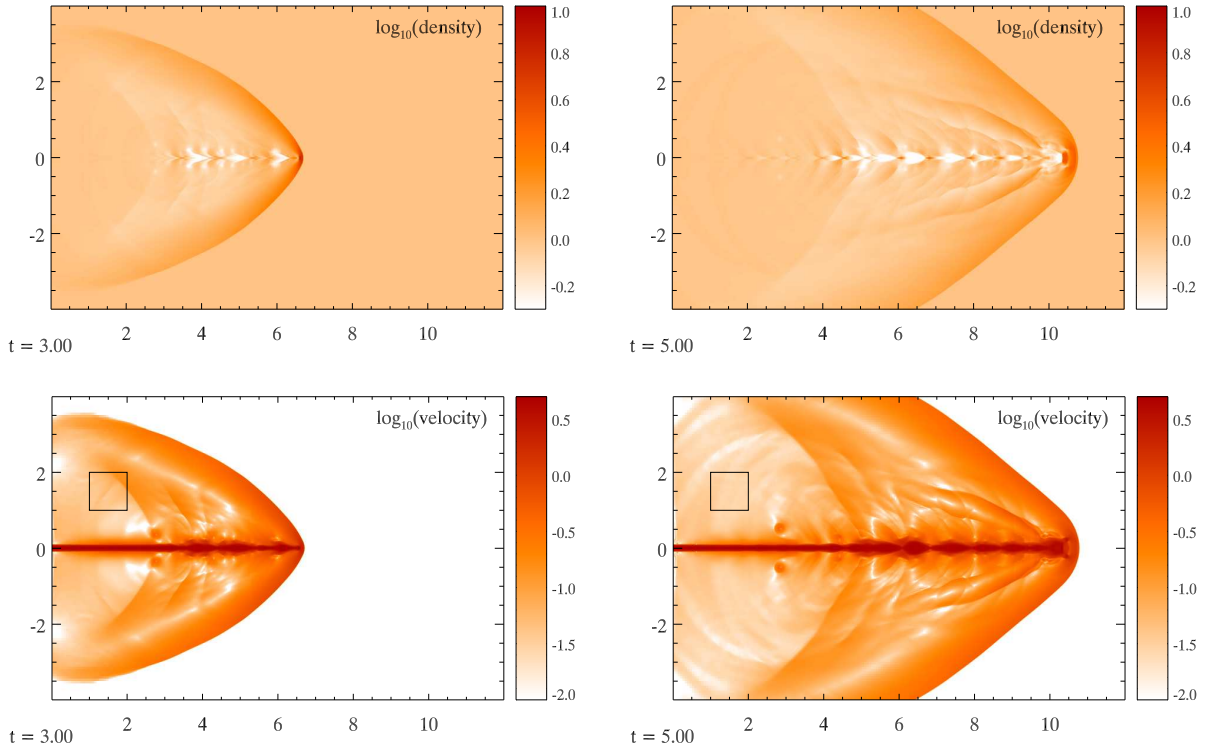


Fig. 1.— Density (top) and velocity (bottom) evolution of a Mach 5 jet (run M5c) at two different times, $t = 3.0$ (left) and $t = 5.0$ (right). The jet is continuously powered and runs into a homogeneous medium. The jet develops knots from reflections off the jet edge. This structure propagates also into the ambient media. Additionally, Kelvin-Helmholtz instabilities develop at the edge of the jet. The turbulent flow outside the jet is mainly subsonic.

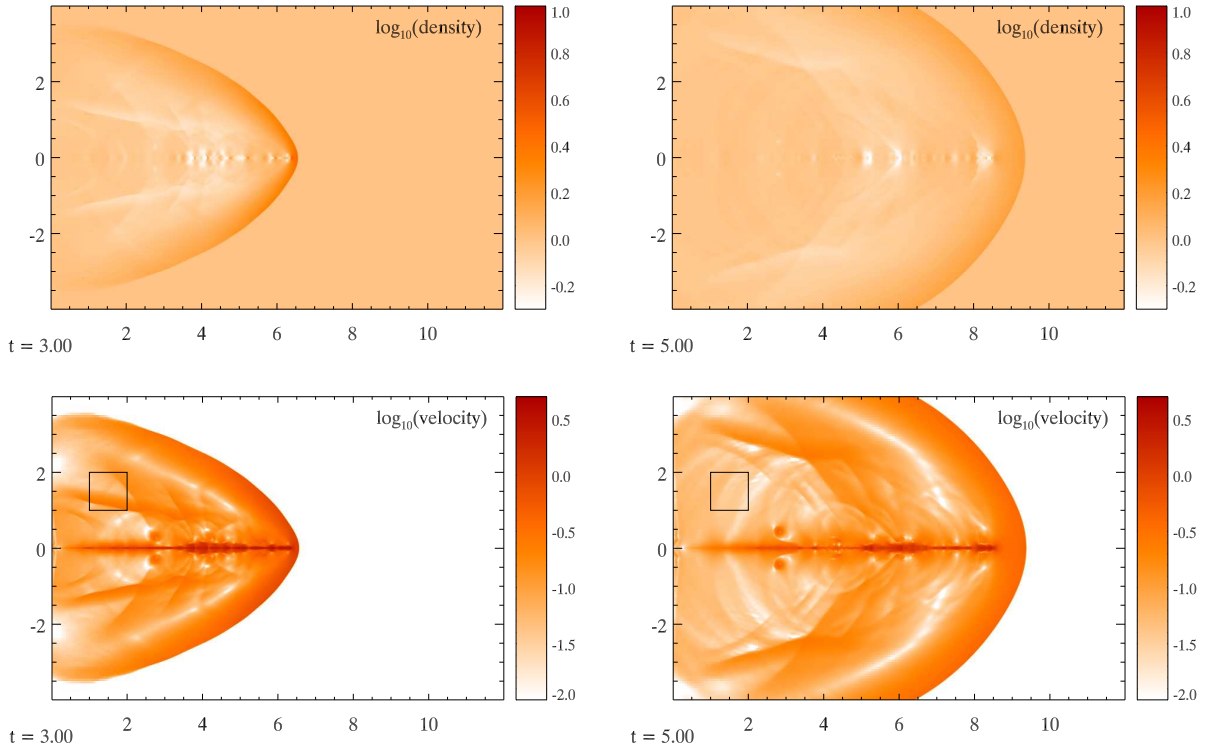


Fig. 2.— Density (top) and velocity (bottom) evolution of a transient Mach 5 jet (run M5t) at two different times, $t = 3.0$ (left) and $t = 5.0$ (right). The jet is shut off at $t = 1.3$ and runs into a homogeneous medium. Compared to the continuously driven jet (cf. Fig 1) the structure at late times (*right panels*) entrained by the jet has already homogenised, an indication of decaying large amplitude fluctuations.

run	dim	Mach	duration	δ	clump	MHD
M5c	2D	5	∞	1	no	no
M5t [g1.4]	2D	5	1.3	1	no	no
M10c	2D	10	∞	1	no	no
M20tCl	2D	20	0.6	1	yes, $\delta_{cl} = 10$	no
M5t3D	3D	5	1.3	1	no	no
M10tOd3D	3D	10	1.3	10	no	no
M10tMpll3D	3D	10	1.3	1	no	yes, parallel field
M10tMpe3D	3D	10	1.3	1	no	yes, perpendicular field

Table 1: Summarises the parameters of the different simulations. We refer to a certain simulation in the text by the name *run*. *Mach* is the Mach number of the jet, where the sound speeds in the jet medium and ambient medium are the same. The jet is driven for the time *duration* in simulation units after which the energy injection is switched off. The density contrast of the jet and possible a clump are given by $\delta = \rho_{jet}/\rho_{amb}$ and $\delta_{cl} = \rho_{cl}/\rho_{amb}$, respectively. Magnetic field runs are denoted by *MHD*, where the homogeneous magnetic field is either parallel or perpendicular to the jet axis. For comparison we show the results of simulation M5t also with a barotropic EOS ($\gamma = 1.4$, M5tg1.4) in all other cases we use an isothermal EOS.

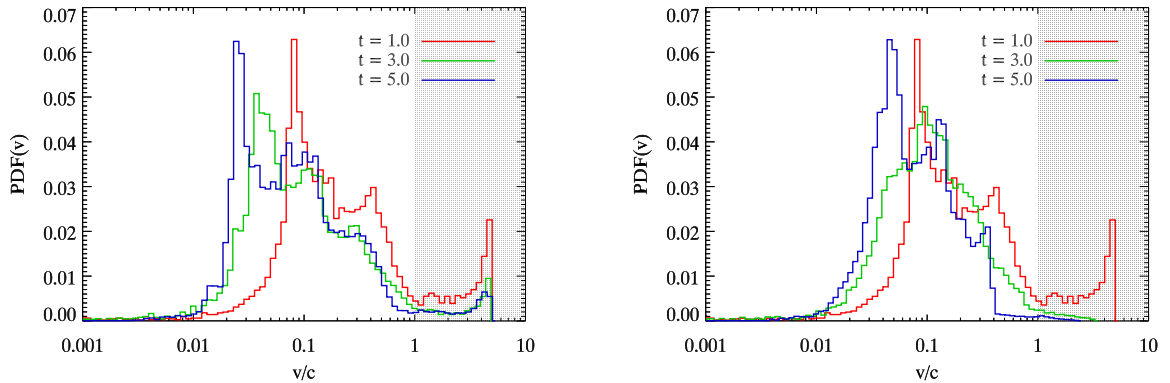


Fig. 3.— Shows the time evolution of the probability density function of velocity fluctuations in the case of an continuously driven jet (*left panel*) and a jet whose engine ceased at $t = 1.3$ (*right panel*). See also Figs. 1 and 2 and text. The amplitudes of the velocity fluctuations are given in units of the sound speed (i.e. as Mach number). The transient jet does not show any significant supersonic fluctuations after the driving has been stopped. Even in the continuously driven case most of the velocity fluctuations are subsonic (less than 2% of the fluctuations are supersonic). Obviously, the peak at $v/c = 5$ comes from the Mach 5 jet itself.

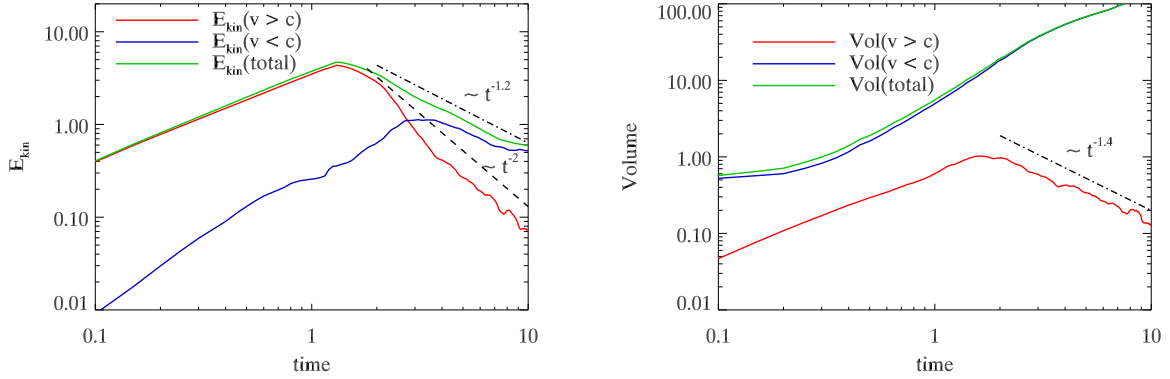


Fig. 4.— Shows the time evolution of the kinetic energies (E_{kin} , *left panel*), and corresponding affected volume (V , *right panel*) for the transient jet M5t. The quantities are divided into a supersonic regime, $v > c$, and a subsonic regime, $v < c$. The decay of supersonic energy contributions is much faster (faster than $\propto t^{-2}$) than the subsonic one. The time shift between the peaks in the kinetic energies shows that the subsonic fluctuations are powered by the decay of the supersonic motions. Unlike the subsonic fluctuations, supersonic motions do not spread after the jet is shut off, as can be seen in the right panel.

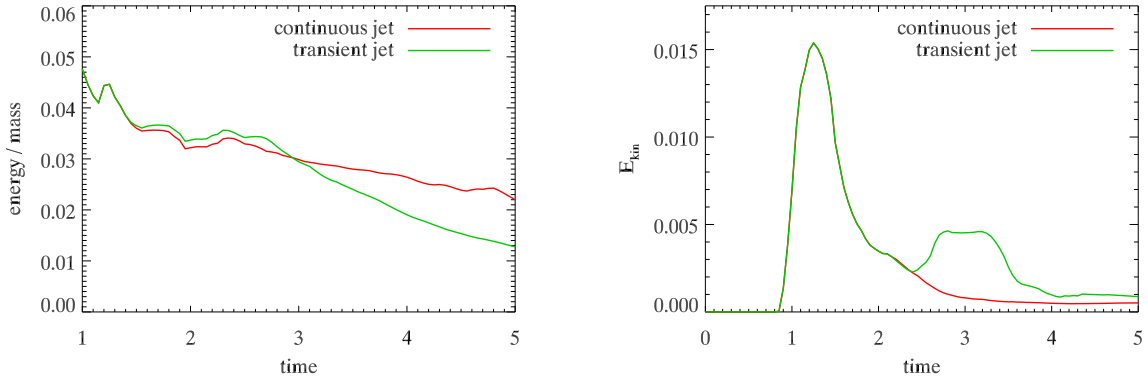


Fig. 5.— Shows the time evolution of the energy for the runs M5c (continuous jet) and M5t (transient jet), respectively. *Left panel*: Kinetic energy per unit mass. Here, we used only contributions from subsonic motions to calculate the energy. The slightly enhanced energy from the transient jet during the intermediate times $1.5 < t < 3.0$ comes from the rarefaction wave travelling from the back-end of the jet. *Right panel*: The total kinetic energy from a region aside the jet (marked as boxes in the images of Figs. 1 and 2). The bump in transient jet case comes again from the rarefaction wave running through this area after the jet is switched off.

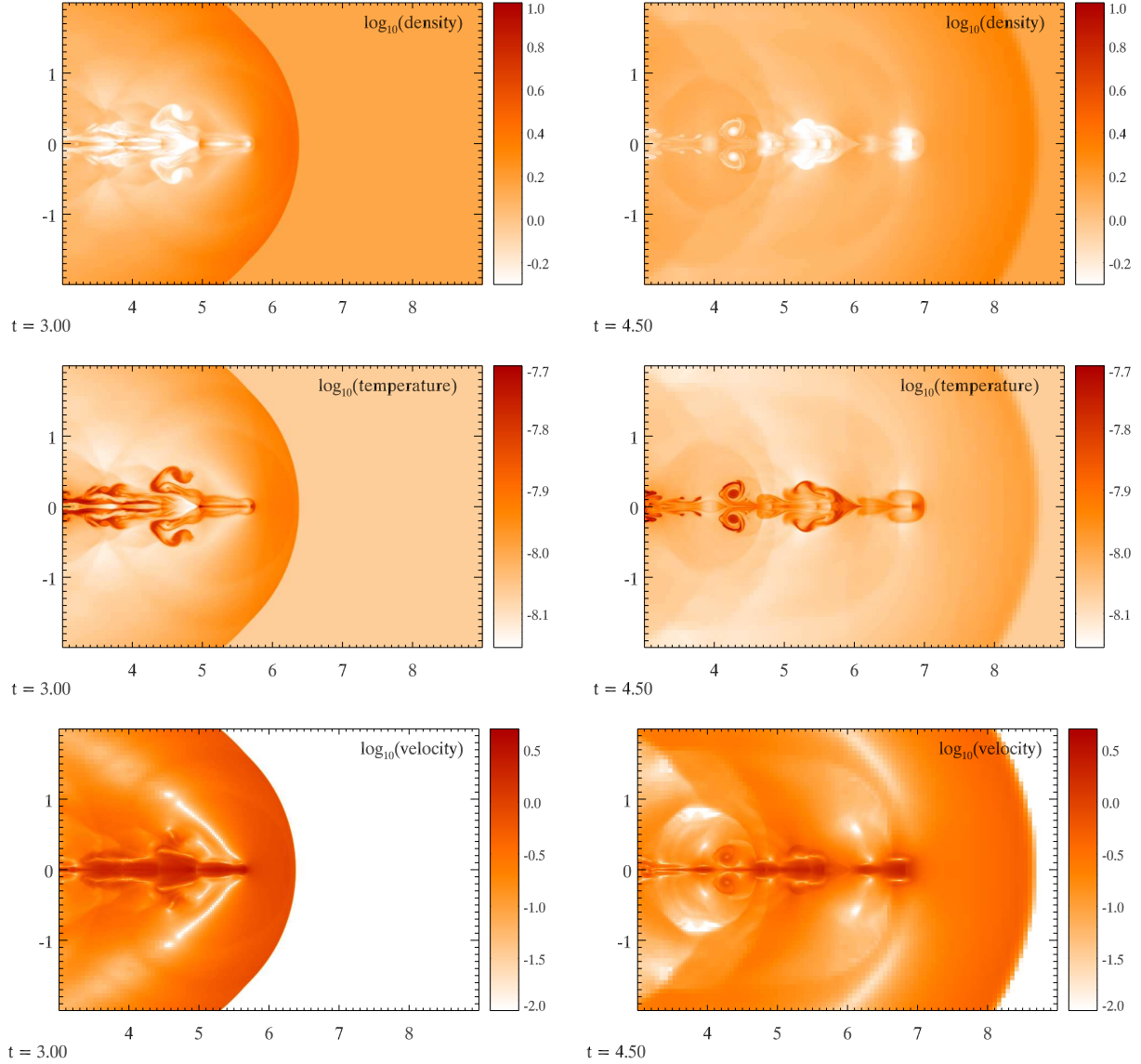


Fig. 6.— Shows the density (top), temperature (middle) and velocity (bottom) evolution of a transient Mach 5 jet (run M5tg1.4) at two different times, $t = 3.0$ (left) and $t = 4.5$ (right). This simulation run is the same than the isothermal run M5t (see Fig. 2) except of the equation of state. Here we use a barotropic EOS (i.e. $p \propto \rho^\gamma$) with a barotropic index of $\gamma = 1.4$. Similar to the isothermal case, instabilities develop at the edge of the jet (seen clearly in the temperature map) but the associated velocity fluctuations are mainly subsonic (cf. Fig. 7).

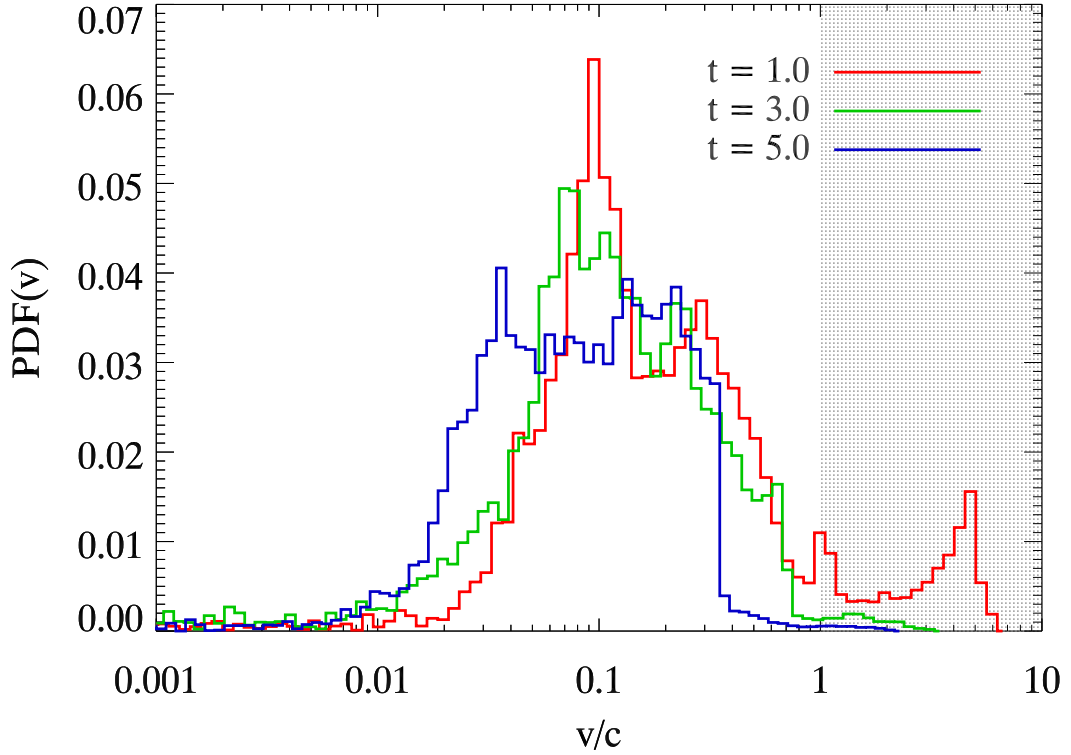


Fig. 7.— Shows PDFs of the velocity fluctuations from the barotropic run M5tg1.4 at different times. This run is similar to the isothermal run M5t (see Fig. 3) except of the equation of state. Here we use a barotropic index of $\gamma = 1.4$. Note that the velocities are scaled to the *local* sound speed. See Fig. 6 for the temperature and velocity structure. Like in the isothermal case, supersonic velocity fluctuations are damped quickly and do not spread far from the jet itself.

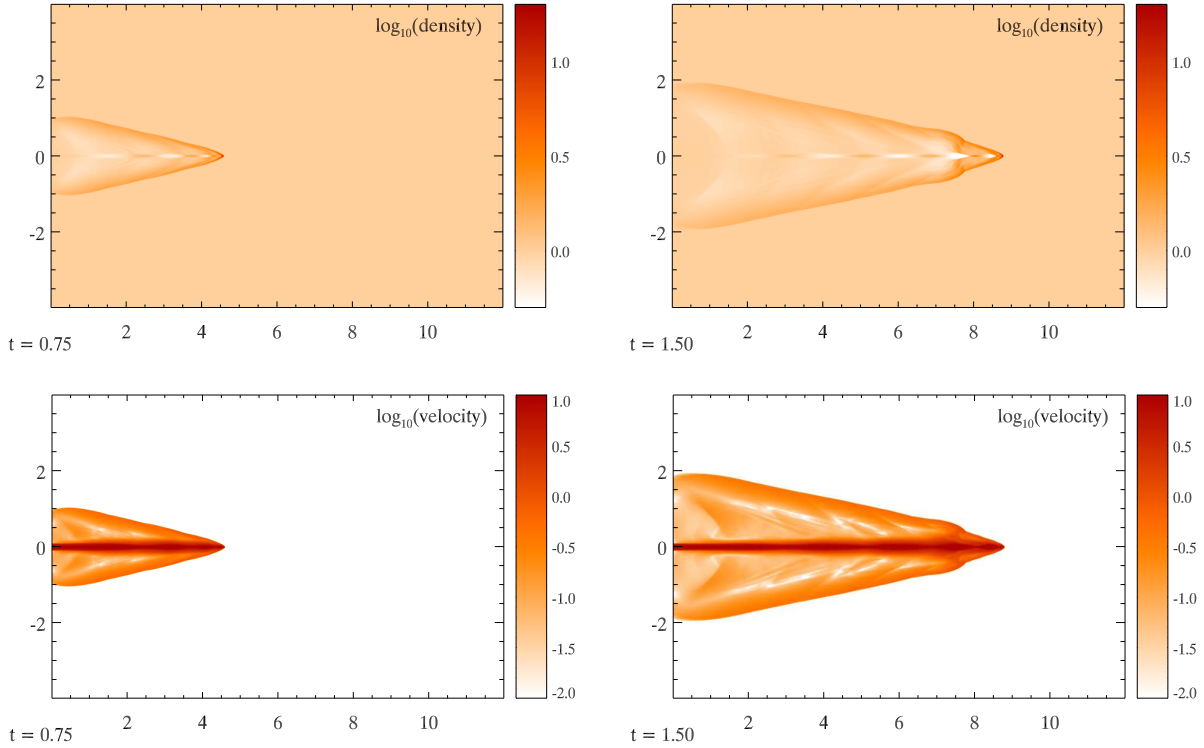


Fig. 8.— Density (top) and velocity (bottom) evolution of a high-velocity Mach 10 jet (run M10c) at two different times, $t = 0.75$ (left) and $t = 1.5$ (right). Compared to the slower Mach 5 jet (cf. Fig. 1) this jet is much narrower and its bow shock radius is smaller, indicating that high velocity jets entrain less gas of their surrounding medium. Apart from very narrow regions around the jet edge and the tip of the bow shock, the excited gas motions are still mainly subsonic (see also Fig. 9).

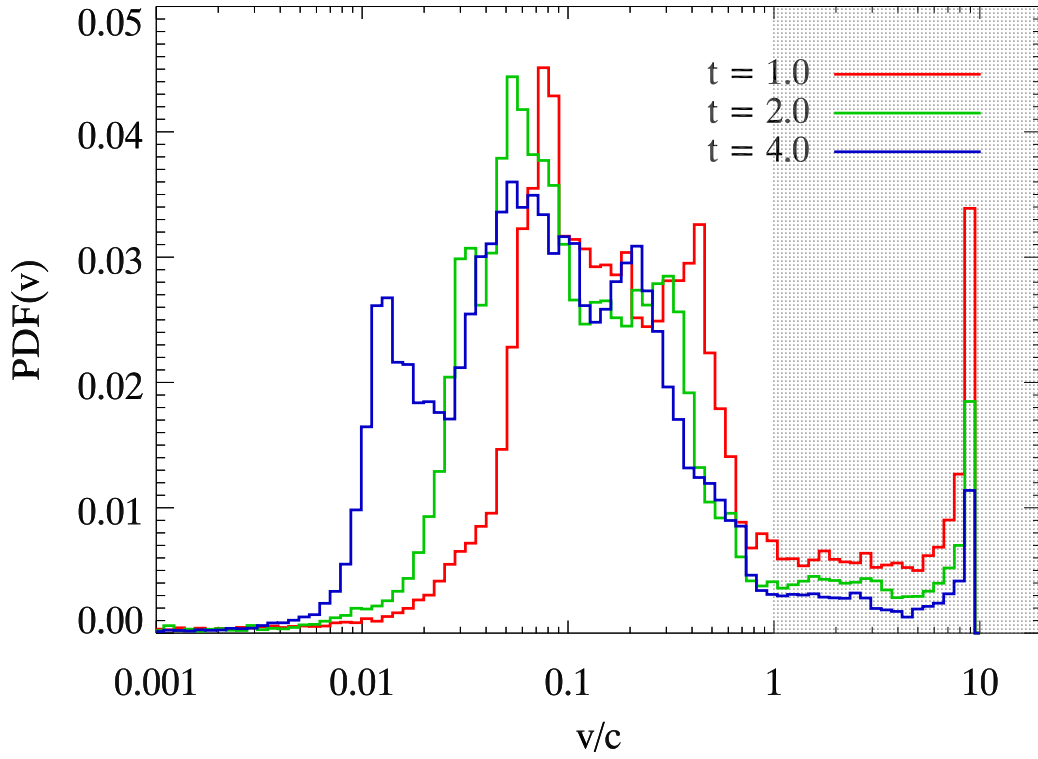


Fig. 9.— Shows the time evolution of the probability density function of velocity fluctuations in the case of the continuously driven Mach 10 jet M10c. The amplitudes of the velocity fluctuations are given in units of the sound speed (i.e. as Mach number). Essentially no supersonic fluctuations get excited by the jet (the peak at $v/c = 10$ is the jet itself).

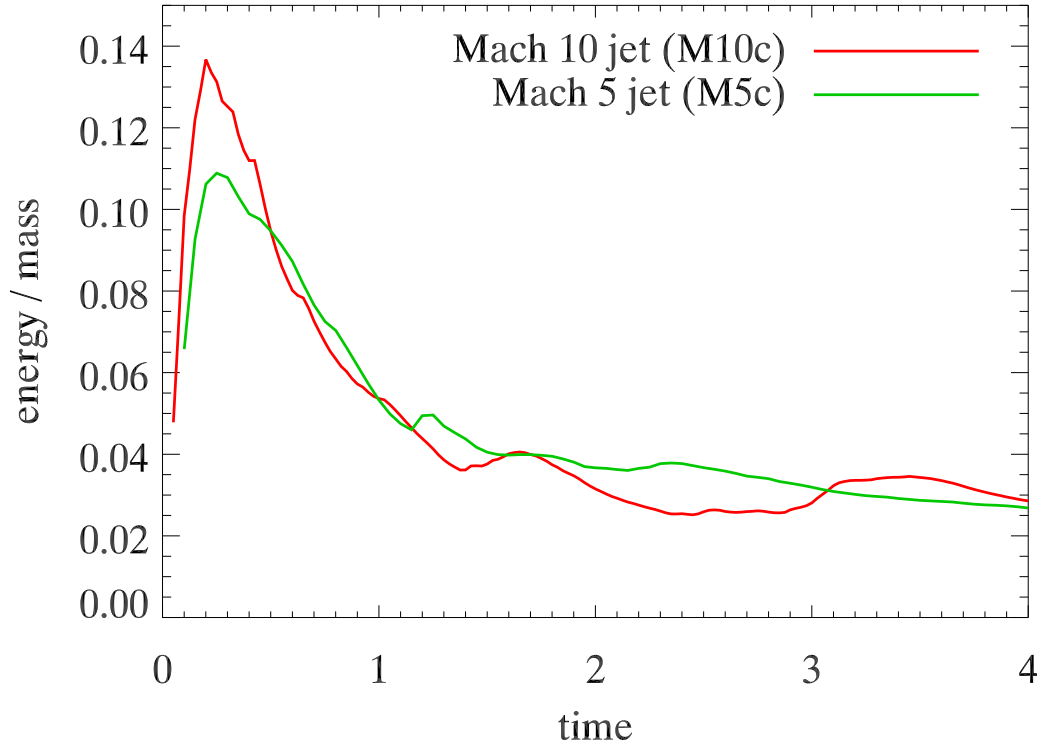


Fig. 10.— Shows the time evolution of the kinetic energy per unit mass, ϵ_{kin} , for the Mach 10 and Mach 5 runs M10c and M5c, respectively. Here, the energy is calculated only for subsonic motions. Despite the larger momentum of the Mach 10 jet it does not excite much larger subsonic velocity fluctuations than its Mach 5 counterpart during the quiescent phase, i.e. at time $t \gtrsim 1.0$.

The knots result from reflection waves off the jet edge where the spacing between them is roughly $2 \times \text{jet radius} \times \text{Mach number}$. The bow shock has a relatively large radius and becomes transonic close to the vicinity of the jet.

Jets from young stellar objects (YSOs) are usually driven for $10^4 - 10^5$ years until the powering engine (disk- or stellar jet) stops working. To study the influence of the end stage of jets we stop driving the jet after a certain time. Fig. 2 shows the time evolution of the density and velocity after the jet was shut off at $t = 1.3$. Compared to the continuously driven jet (see Fig. 1) large velocity and density fluctuations have already decayed, the bow shock has slowed down, and its radius increased as expected for a slower moving jet. On the other hand, the rarefaction wave travelling from the end of the jet excites (low amplitude) fluctuations in the gas. This is particular important if this pressure wave travels through a clumpy medium as we will see later in this text.

From Fig. 3, which shows the velocity PDFs for the runs M5c and M5t, one can see that only a small fraction ($< 2\%$) of the excited fluctuations are supersonic. The majority of the motions are subsonic, with most around a Mach number between 0.03 and 0.1. Even in the case of a continuously driven jet, the peak of the PDF moves towards smaller fluctuations with time, which shows that high amplitude fluctuations decay quickly.

One of the most interesting features apparent in the PDFs is that supersonic fluctuations close to the jet drop quickly and occupy only very little volume until the excitation becomes subsonic (following the PDF from the jet position at $v/c = 5$ to the left). Only subsonic motions get excited distinctly¹. This shows that supersonic fluctuations do not propagate far from the jet itself, and that second-order excitations are always subsonic. This low plain in the PDFs between the jet peak and the sonic point can be regarded as the *supersonic desert*. Here, the jet is not able, although continuously driven, to excite a large fraction of supersonic motions in the gas. Supersonic fluctuations are highly compressive and their energy is mainly consumed in compressing the gas instead of pushing the gas to high velocities. The expansion of the compressed gas, in turn, excites only *subsonic* fluctuations. This is the reason for the 'supersonic desert' between the jet peak and the transonic regime. The subsonic fluctuations are largely incompressible and can propagate far into the medium. Given enough time, these subsonic fluctuations will occupy most of the excited gas, so the PDF peaks deeply in the subsonic regime.

The right panel of Fig. 3 (transient jet) shows clearly the decay of supersonic motions with time. The highest velocity fluctuations, in particular the supersonic ones, are the fastest damped ones. This can also be seen in Fig. 4 where we show the time evolution of the kinetic energy for the supersonic and subsonic regime separately. The contributions from supersonic motions to the kinetic energy decay much faster than the subsonic ones. The former contributions decay as quickly as $\propto t^{-2}$ which should be compared to the decay of subsonic fluctuations which follow a

¹Note that the absolute decline of the jet peak in the PDFs of continuously driven jets is due to our choice of sampling. Here, the sampling volume increases as the jet-affected regions increases with time.

power law $\propto t^{-1}$. Nevertheless, the total energy decays as $\sim t^{-1.2}$ which is in agreement with previous studies of decaying supersonic turbulence (e.g. Mac Low et al. 1998; Mac Low 1999). Evidently, supersonic fluctuations do not excite further supersonic motions in their neighbourhood. Instead their momentum is mainly transferred into subsonic compressional modes. Unlike subsonic fluctuations which spread into an ever increasing region, the supersonic ones do not propagate into a larger volume. This can be seen from the evolution of the affected volume in both cases (see right panel of Fig. 4).

In the transient jet case, essentially all supersonic fluctuations decayed after one sound crossing time over the size of the fluctuations. Again, this is expected as supersonic fluctuations decay quickly and do not propagate far into the ambient medium. At $t = 5$ the main fluctuations peak at slightly higher amplitudes than in the continuously driven case ($v \sim 0.05$ instead of $v \sim 0.025$). This is due to motions excited by the rarefaction wave travelling from the back end of the jet into the ambient medium. This feature is illustrated in Fig. 5 where we compare the time evolution of the energy from the continuous and transient jets, M5c and M5t, respectively. Although the transient jet is switched off at $t = 1.3$, its energy per unit mass², ϵ_{kin} , exceeds that of the continuous jet beyond this time until $t \sim 3.0$. We therefore conclude that transient jets are more capable of driving turbulence, albeit only in the subsonic regime.

Although a typical PDF has one or two peaks in the subsonic regime, these features are not due to the bow shock. We tried to identify typical features of the jet in the PDF but, apart from the jet itself, others do not stand out in the distribution. The bow shock region does not occupy a large volume fraction.

In one case (run M5tg1.4) we also varied the EOS of the gas using a barotropic relation with $p \propto \rho^{1.4}$. This gas behaviour mimics the inefficient cooling ability in the optical thick regime. The run M5tg1.4 should be compared to the isothermal simulation M5t, which otherwise has the same runtime parameters. In Fig. 6 we show density, temperature, and velocity maps at two different times. Like in the isothermal case Kelvin-Helmholtz instabilities develop at the edge of the jet which are best seen in the temperature map. Otherwise, the bow shock radius is larger in the non-isothermal case reflecting additional thermal effects and a higher sound velocity. Nevertheless, the high amplitude fluctuations are also damped quickly (see Fig. 7) and are not found far from the jet.

The influence of the jet speed on the environment can be seen in Fig. 8 where we show the evolution of a Mach 10 jet (run M10c). The first feature one notices is the narrowing of the bow shock region compared to the slower jet (run M5c). This shows that a faster jet entrains less volume than a slower one. Therefore we conclude that high Mach-number jets leave less imprint on their environment than their slower counterparts, as long as they do not become unstable.

²Here we show the energy per unit volume, i.e. $\epsilon_{\text{kin}} = 1/2 \int dV \rho v^2 / M$ with $M = \int dV \rho$, to account for the fact that material can leave the simulation box. The integration volume, V , is the regime affected by subsonic fluctuations, i.e. $V_{\text{sub}} = V(0 < v < c)$.

This is also corroborated by the fact that supersonic motions do not propagate far from the jet. Furthermore, high-velocity jets are more stable than low Mach-number jets and are less likely to develop instabilities. Therefore, high-velocity jets will stay collimated for a longer time and a larger distance, which in turn reduces the volume entrained by the jet. From the velocity PDF of this jet (Fig. 9) one can see that the supersonic desert occupies a larger velocity range in the case of a faster jet (cf. Fig. 3) which shows again that the supersonic velocity fluctuations are strongly suppressed compared to the subsonic fluctuations because supersonic fluctuations do not persist long and are not excited far from the jet itself. Rather, the energy of supersonic modes is transferred from large to small scales abruptly in a network of shocks (Smith et al. 2000).

Observations also support the typical velocity structure seen in our simulations. For instance, strong velocity gradients where the speed declines quickly in the direction off the jet axis are seen in the HH21 jet observed by Gueth & Guilloteau (1999).

Comparing the kinetic energy evolution of the Mach 5 and Mach 10 jets one sees from Fig. 10 that even in the subsonic regime the higher velocity jet does not deposit much more energy into the ambient medium. In this figure we show again the time evolution of the kinetic energy per unit mass, ϵ_{kin} . After an initial ramp-up phase (until $t \sim 0.3$) the energy contained in the subsonic regime starts to 'decay' because more and more gas, i.e. mass, is entrained (note that both jets are continuously driven). Shortly after the peak is reached, the energies in the fast and slower case become of similar strength showing that the relative impact of high velocity jets is not greatly enhanced compared to their slower counterparts.

To compare our above presented slab jet simulations with more natural configurations we performed a series of three-dimensional jet simulations with similar setups. Although the study of two-dimensional slab or axis-symmetric jets is instructive and the results represent the gross features of jets, jets in three dimensions have more degrees of freedom and can therefore develop more instabilities but generally pervade a smaller fractional volume than in two dimensions.

In Fig. 11 we show a time sequence of the velocity PDFs from the 3D run M5t3D. This setup should be compared to the two dimensional slab jet of run M5t where both have a speed of Mach 5 and are driven until $t = 1.3$. As expected, the volume filling factor of the jet (i.e. the supersonic regime) in the 3D case is much smaller than in the 2D setup. Apart from this fact the two cases evolve quite similarly. Differences show up in particular instabilities at the jet surface. For instance the Kelvin-Helmholtz instabilities appear on smaller scales in the 3D case.

Finally we mention that we did not investigate rotating jets. Jet rotation is indicated in some sources with micro jets (see e.g. Bacciotti et al. 2002; Ray et al. 2007) and can be fitted in principle by magnetohydrodynamic models of jet formation in order to derive the launching radius of the jet (see e.g. Anderson et al. 2003; Fendt 2006; Pudritz et al. 2007). Typical rotational velocities (if existent) are about a factor 10–100 times smaller than the jet bulk speed. It is unlikely that such a small velocity shear to the ambient medium may launch supersonic turbulence. However, rotating jets may be affected by additional modes of instability, and thus may give rise to a different overall

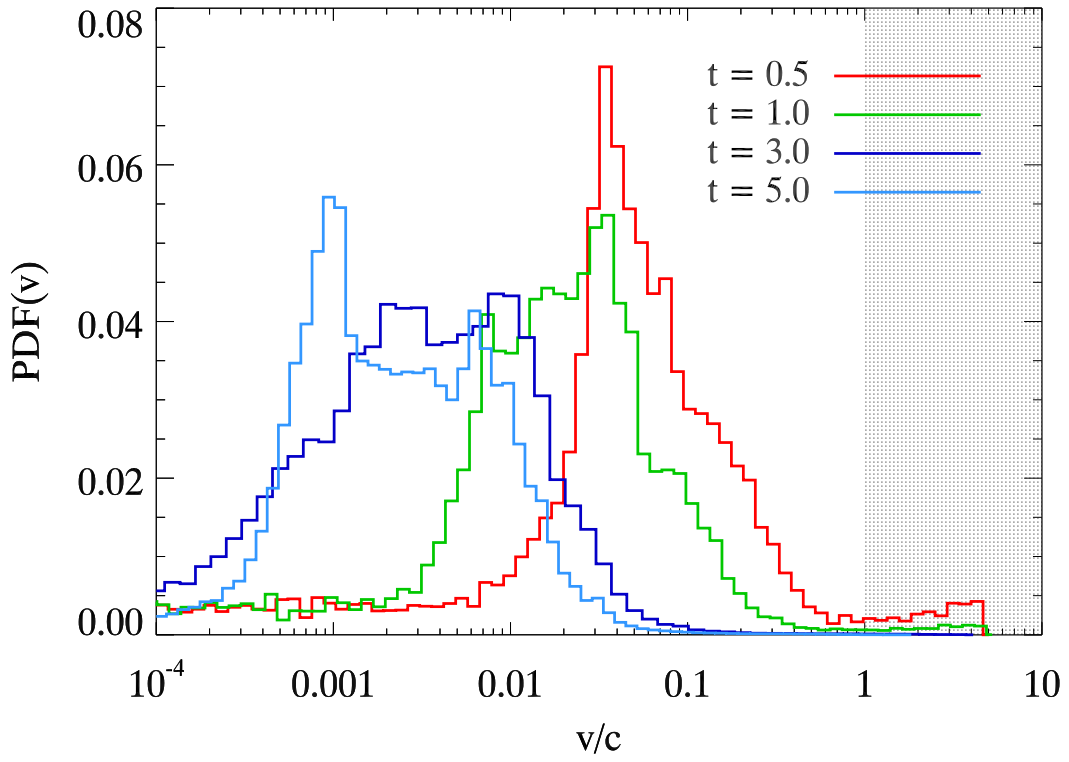


Fig. 11.— Shows a time sequence of the velocity PDF from the three-dimensional run M5t3D. Compared to the 2D runs the filling factor of the jet ($v/c = 5$) and the supersonic regime decreased significantly due to the increased degrees of freedom of velocity excitations.

turbulence pattern. We will investigate this important aspect in a forthcoming paper.

3.2. Jet–Clump Interaction

The environment in which jets are launched is usually non-homogeneous, i.e. clumpy and often stratified. Early studies of outflows interacting with a stratified environment (a density gradient in the ambient media) showed that the morphology of the jet’s bow shock changes significantly in such a situation (Henney 1995). More dramatically, jets will be deflected if they hit a high-density obstacle with a certain inclination angle (e.g. Raga & Canto 1995; de Gouveia Dal Pino 1999).

Here, we model a scenario of jet–clump interaction with a Mach 20 jet running into an overdense spherical region, where the density contrast between clump and ambient medium is $\delta_{\text{cl}} = 10$ (here, the jet density equals the density of the ambient medium). The ratio of the clump radius to the jet radius is 7.5 (run M20tCl). Furthermore the jet driving is switched off at $t = 0.6$. Fig. 12 shows the density and velocity of this jet–clump interaction simulation before ($t = 0.25$) and after ($t = 2.5$) the driving engine ceased. Initially the high Mach number jet runs through the clump without a large influence. Even the bow shock is very narrow inside the overdense region and leaves only a small trace of compressed gas at the edge of the jet. The bow shock starts to expand again in the low density region after the jet leaves the clump (not shown in the images). Essentially a high Mach number jet acts like a bullet penetrating a clump of material. Again, the situation changes after the jet engine stops: a rarefaction wave travels from the back end of jet into the ambient medium. This pressure wave produces the main disturbance in the clump and excites large instabilities at the clump’s edge. The instabilities develop to Rayleigh-Taylor fingers which move into the low density medium. In the particular case here (2D slab jet, no self-gravity) the clump is entirely dispersed by the transient jet. This shows again that high-velocity jets have a large impact on their environment and might even disrupt entire cloud cores, but they are unlikely drivers of supersonic turbulence in a large fraction of the molecular clouds. Fig. 13 shows a time sequence of the velocity PDF in the case of this jet (M20tCl) which indicates a rapid decay in time and amplitude of supersonic turbulence.

3.3. High-Density Jets

Jets from YSOs seem to pass through different evolutionary stages. In particular, the youngest jets show evidence of containing high density gas with $n(\text{H}_2) > 10^5 \text{ cm}^3$ (see review Reipurth & Bally 2001, and references herein). The density within these jets exceeds the mean density of their surrounding media. Such high-density jets have the potential to leave a larger imprint in the ambient medium than their lower density counterparts as they carry more momentum.

In Fig. 14 we show images of the density and velocity of an overdense ($\delta = 10$, Mach 10) jet-simulation. One of the striking features of this jet is that the beam-width of the jet increased

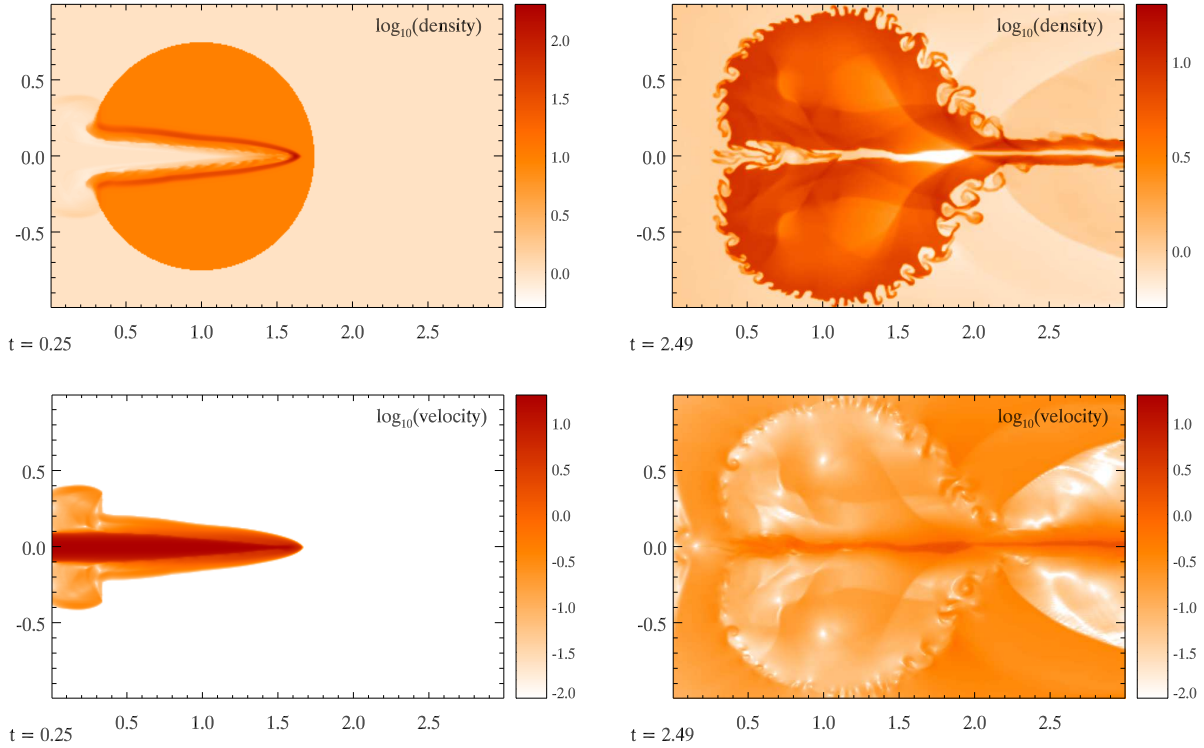


Fig. 12.— Jet–Clump interaction. Shown are the density and velocity distribution of a Mach 20 jet at two different times, $t = 0.25$ (left) and $t = 2.5$ (right). The earlier stage shows the situation while the jet is still powered whereas the jet powering has ceased in the later stage (shut off at $t = 0.6$). The imprint from the jet is clearly visible in the clump structure even at much later stage but the velocity fluctuations are subsonic. Note that the simulation box is much larger than shown here (box size: 24×8)

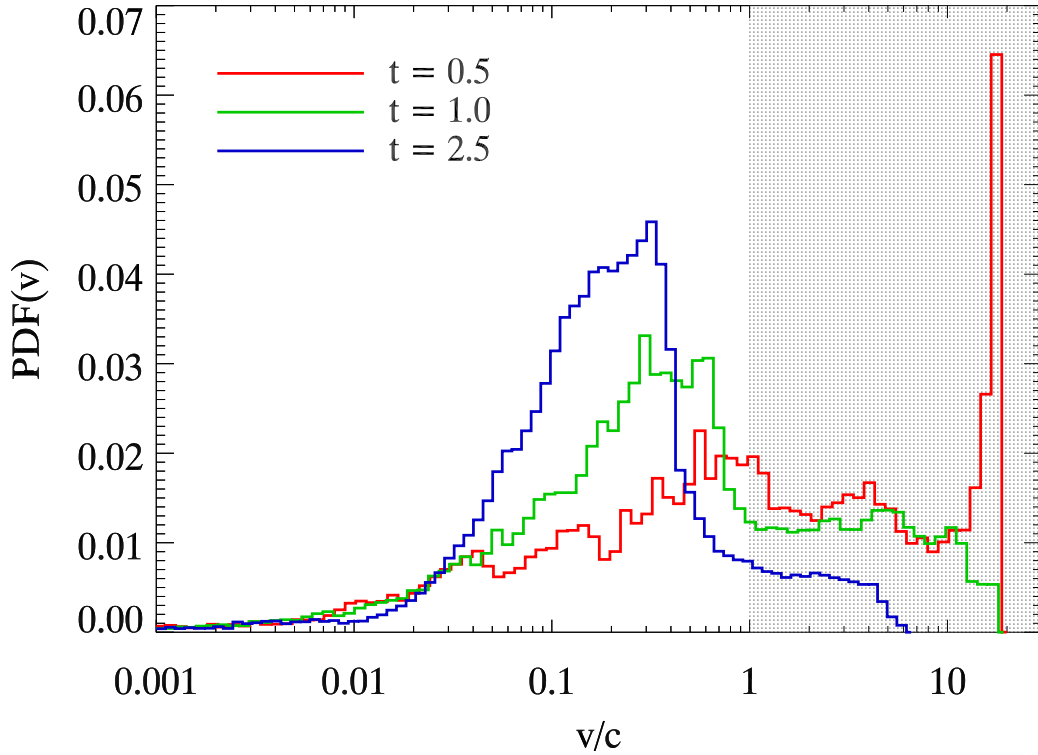


Fig. 13.— Shows a time sequence of velocity PDFs in the case of the transient Mach 20 jet M20tCl interacting with a dense clump. The peak at $v/c = 20$ is due to the jet itself. Here again, supersonic velocity fluctuations are not copiously excited and are damped quickly after the jet driving engine ceased at $t = 0.6$. Nevertheless, the clump is strongly disrupted by the jet and might even fully dissolve after some time (see Fig. 12)

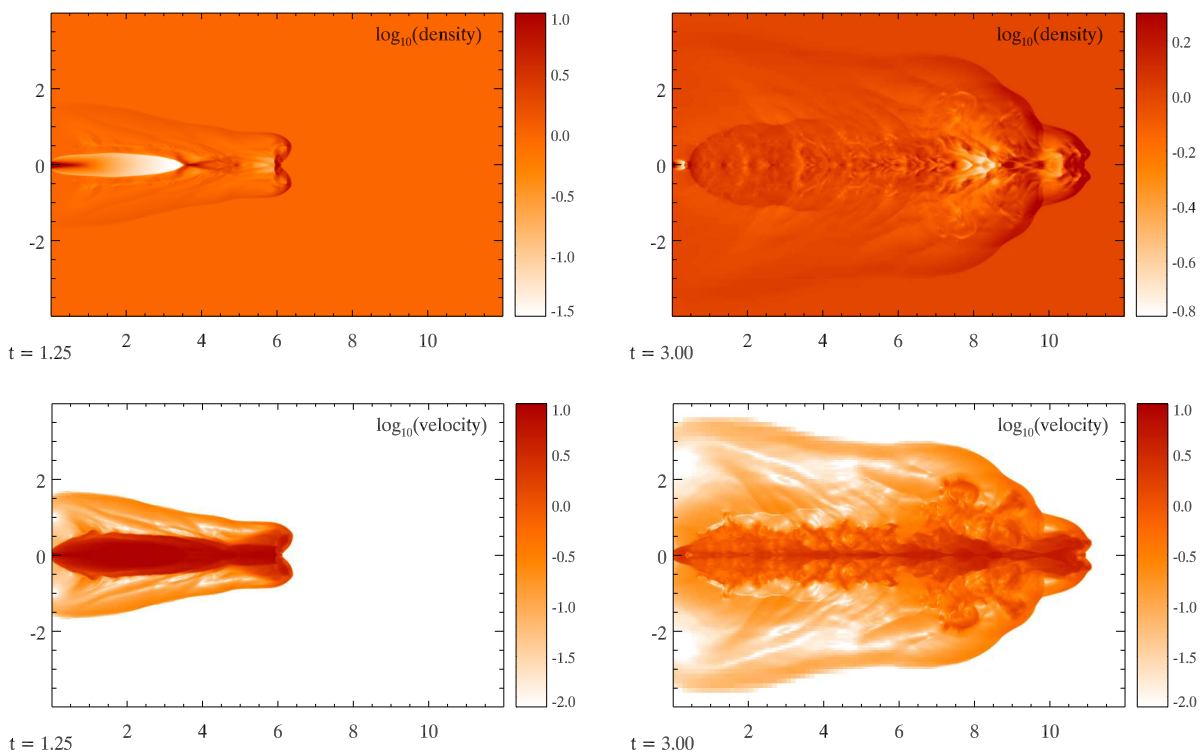


Fig. 14.— Shows 2D cuts through the density (top) and velocity (bottom) of the 3D simulation M10tOd3D (Mach 10, overdense jet) at two different times, $t = 1.25$ (left) and $t = 3.0$ (right). The beamwidth is wider and the bow shock region is distinctively different in this case than in the case of an equal density jet (cf. Fig. 8)

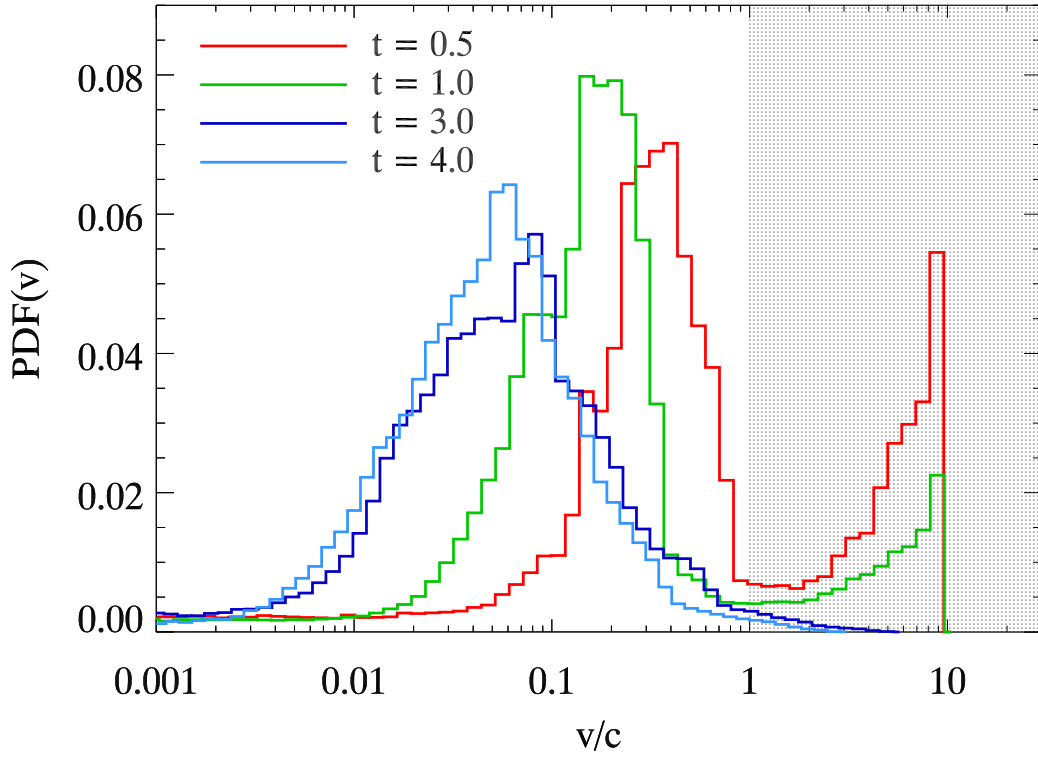


Fig. 15.— Shows a time sequence of the velocity PDF from the three dimensional, overdense jet M10tOd3D before and after the driving engine is turned off at $t = 1.3$. A larger fraction of the excited fluid motions is supersonic in this overdense-jet case but the supersonic excitations decay quickly again after the jet driving is shut off at $t = 1.3$.

by a factor of a few (lower left panel of Fig. 14). At the foot-point the jet has a diameter of 0.2 in simulation units and increases to ~ 1.0 at a distance of ~ 1.0 . This broadening of high-density jets helps to pervade a larger volume fraction and excite high amplitude velocity fluctuations. Note that this jet is not in pressure equilibrium with its surroundings, which means that the amount of excited motions due to the jet expansion is an upper limit to the possible impact of overdense jets. In Fig. 15 we show a sequence of velocity PDFs of this overdense jet before and after the jet’s engine ceased at $t = 1.3$. Although the supersonic wing decreases steeply from the jet peak at $v/c = 10$ its slope is not as steep as in the case of an equal density jet (cf. Fig. 9). As long as the overdense jet is powered supersonic motions make up a significant fraction of the excited gas velocities but get damped quickly again after the driving stopped.

Another interesting feature of the overdense jet is the shape of the bow shock. The overdense jet shows strong sideway motions due to the higher pressure inside the jet which effectively de-collimates the jet and increases the bow shock region forming a cone-like shape at the tip of the jet.

3.4. MHD Jets

Magnetic fields are observed in a variety of molecular clouds cores (e.g. Crutcher et al. 1999) and may exist in all of them. Additionally, jets are most probably magnetically launched and collimated phenomena (e.g. Blandford & Payne 1982; Pudritz & Norman 1983; Ouyed & Pudritz 1997; Fendt & Čemeljić 2002). Here, we study the influence of background magnetic fields on the jet-driven turbulence by two configurations: First we set up a homogeneous field parallel to the jet axis (run M10tMpl3D), and secondly, we rotate this field by 90 degrees which is then perpendicular to the jet axis and aligned with the y -axis of our simulation box (run M10tMpe3D). The magnetic field strength in both cases is set so that the Alfvén velocity, $v_A = B/\sqrt{4\pi\rho}$, equals the sound speed, i.e. $v_A = c$, or in other words the plasma β -parameter is $\beta = p_{\text{therm}}/p_{\text{mag}} = 2$. As the jet is supersonic with a sonic Mach number of $\mathcal{M} = 10$ it is also super-Alfvénic with an Alfvén Mach number of $\mathcal{M}_A = 10$. Initially the fast magnetosonic speed is $\sqrt{2}c$ which is exceeded by the jet. Note that these numbers are defined to the external medium and measure the jet energetics in comparison to the jet environment. The internal dynamics of the jet is defined by the internal Mach numbers. Typical protostellar jets are in rough energy equipartition and have internal fast magnetosonic Mach numbers of about 3.

Interestingly, information along the jet axis is transferred by different wave modes. In the first case where the field is aligned with the jet, Alfvén waves will be able to travel along the jet. In the second case, fast magnetosonic waves will travel across the field in direction of the jet axis. Of course the internal Mach numbers may drastically change during the evolution of our simulation. In particular, in the second case, the parallel field will be highly compressed by the jet (see below), increasing the field strength and thus the Alfvén speed. The jet front will be in a magnetic energy dominated region and the strong field will finally stop the jet propagation.

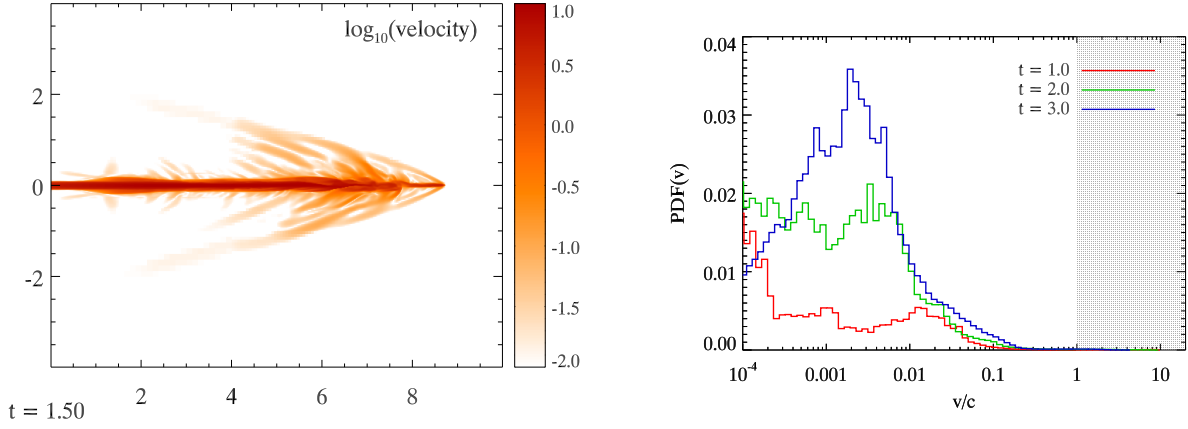


Fig. 16.— Show the velocity structure and a time sequence of velocity PDFs from simulation M10tMpll3D. In this magnetised case (magnetic field parallel to the jet) velocity fluctuations are strongly suppressed compared to the non-magnetised jets (see, for example, Fig. 8).

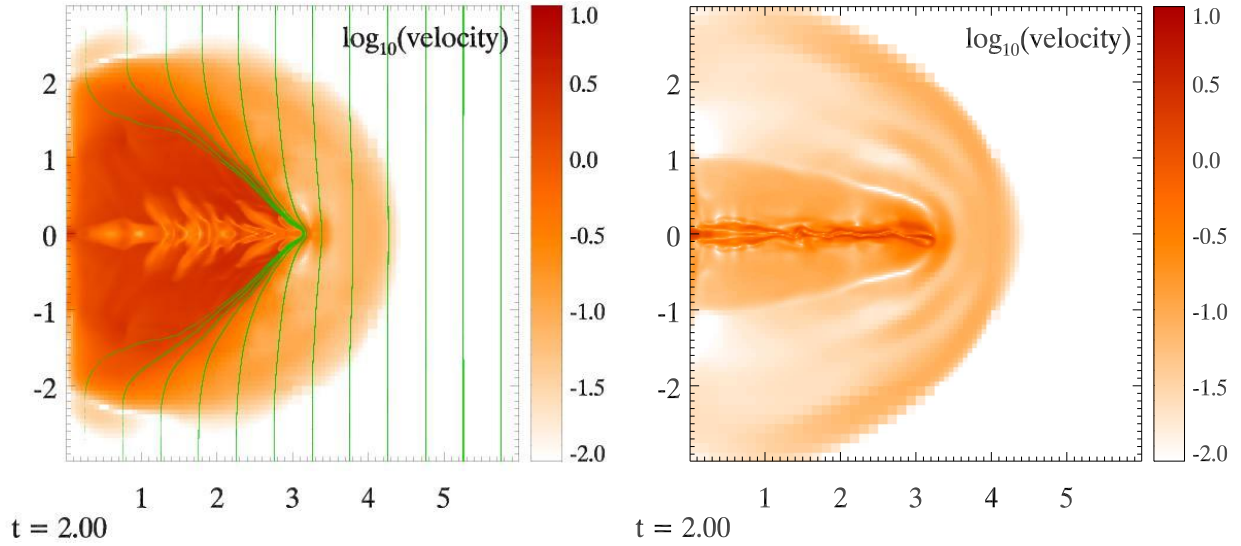


Fig. 17.— Shows the velocity structure form simulation M10tMpe3D (initial homogeneous magnetic field perpendicular to the jet axis). The left panel shows the speed distribution in a 2D slice through the xy plane and the right panel is an image through the xz plane. The jet compresses and distorts the magnetic field whose pressure and tension accelerates gas off the jet axis as seen in the left panel.

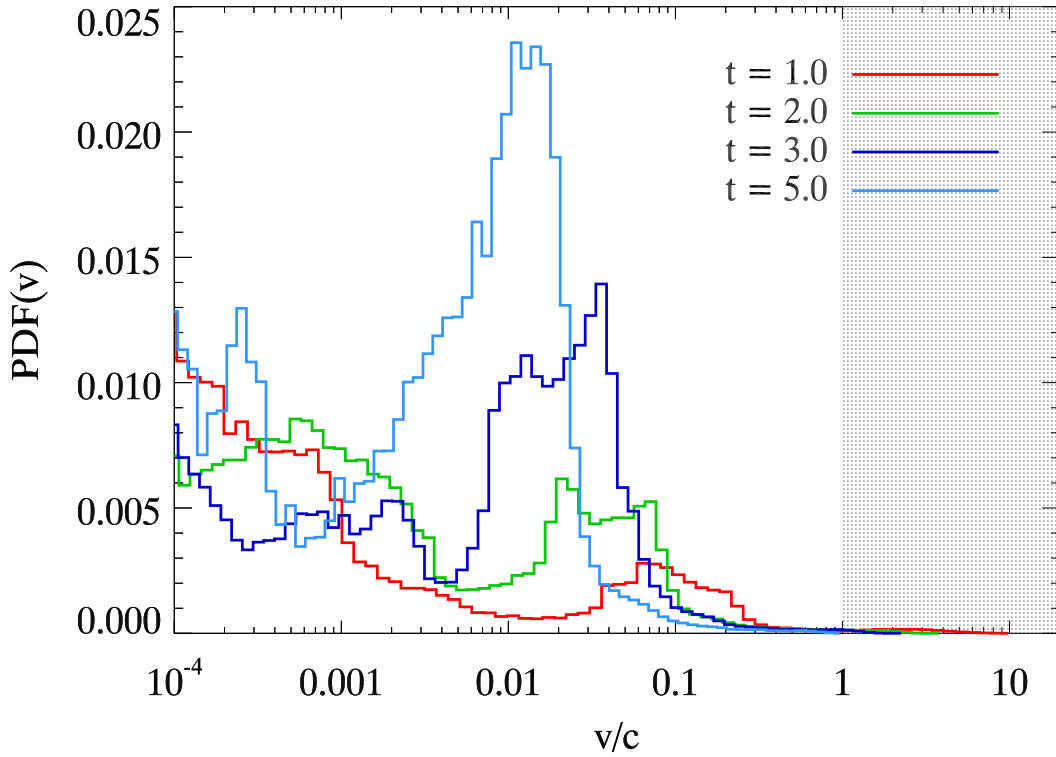


Fig. 18.— Shows a time sequence of the velocity PDF from the MHD jet simulation M10tMpe3D (jet with an initially perpendicular magnetic field) before and after the driving engine is turned off at $t = 1.3$. Although fluid motions are excited along the magnetic field lines (see left panel of Fig. 17) the majority of these velocity excitations are subsonic. Compared to the case of an aligned magnetic field (run M10tMpl3D) the peak of fluid excitations appear at higher amplitudes (cf. Fig. 16). This high amplitude motions are excited by the conversion of magnetic energy into kinetic energy, i.e. by the straightening of the magnetic field lines.

In Figs 16 – 18 we summarise the results of these two simulations. From the velocity structure and its PDF (Fig. 16) one can see that the aligned magnetic field suppresses large amplitude fluctuations. This result is obvious as transverse modes are more difficult to excite due to the additional magnetic pressure in this direction. Furthermore, the jet is more collimated and its bow shock radius is smaller than in the non-magnetic case (cf. Fig. 8). Any excited fluid fluctuations are also damped more quickly in the magnetic case, but have the potential to travel further than in the non-magnetised case. Transverse motions distort the magnetic field lines which in turn counteract the fluctuations leading to damped motions. Longitudinal or Alfvénic excitations can travel (almost) undamped but are unlikely to excite supersonic fluid motions (e.g., Heitsch & Burkert 2002).

Such a scenario can be seen in Fig. 17 where the magnetic field is perpendicular to the jet axis. First, the active jet bends the magnetic field strongly while building up a large component parallel to the jet axis. This parallel component has a large gradient along the former field direction along the y axis. The strength of this effect is of course exaggerated by our assumption of ideal MHD. Real jets will be magnetically diffusive and thus allow the field to penetrate the jet. However, our toy model demonstrates how the built-up magnetic pressure gradient pushes the gas away from the jet axis (see left panel of Fig. 17). This happens only in the direction of the initial field. Perpendicular to it, this magnetic pressure component is negligible and does not accelerate the gas (as seen in right panel of Fig. 17). Additionally, the tension of the stretched magnetic field works against the jet motion and decelerates the high velocity flow. This effect is particularly effective after the driving engine stops and even pushes gas backwards after a while. Obviously the jet does not propagate as far if a perpendicular background field is present. Note that the tension of the bent magnetic field lines also has a force component perpendicular to the jet and helps accelerating ambient gas away from the jet.

In summary, such a field configuration helps to excite higher-amplitude, though still subsonic, fluctuations compared to an aligned magnetic field. The PDFs shown in Fig. 18 shows the peaks of excitations at late times in the amplitude range $v/c \sim 0.01 - 0.1$ whereas the peaks in the aligned case appear at $v/c \sim 0.005 - 0.01$. Note that the Alfvén velocity is initially equal to the speed of sound which in turn means that supersonic velocity fluctuations are also super-Alfvénic.

4. Summary and Conclusion

In this work we presented a detailed study of feedback from protostellar jets based on two and three dimensional ideal HD and MHD simulations of a single supersonic jets in an ambient medium. We focus on the particular velocity and energy structure excited by the jet. Essentially, we used a statistical measure of velocity, namely the velocity probability density function (PDF) to quantify the main contributions to the excited motions, as subsonic or supersonic. The distinction between sub- and supersonic fluctuations is a natural outcome of our investigation: Supersonic motions decline rapidly in velocity space (e.g. Figs. 3 and 9) and do not propagate far from their driving

source. They damp quickly because they excite mainly compressive modes. The re-expansion of the compressed overdensities drives mainly subsonic velocity fluctuations that then propagate further into the ambient medium. Despite the appearance of bow shocks and instabilities, jets do not entrain large volumes with supersonic speeds. In particular, instabilities such as Kelvin-Helmholtz modes at the edge of the jet, develop most efficiently for transonic or slower velocities. High-velocity jets, on the contrary, are bullet-like and stay very collimated, transiting the surrounding cloud without entraining much of its gas (e.g. see Figs. 8 and 12). From the point of view of jet-driven supersonic turbulence in molecular clouds this is a dilemma which is difficult to circumvent. Even in the case of overdense jets which affect more gas of the surrounding media and have higher momenta, the supersonic motions do not propagate far from their source as can be seen in the PDF of Fig. 15.

We also tested the influence of magnetic fields on the jet propagation and jet feedback. Naturally, jets stay more collimated if the magnetic field is aligned with the jet axis and therefore entrain less gas. Furthermore, perpendicular motions are damped by magnetic tension preventing a large spread of high amplitude fluctuations (see Fig. 16). Perpendicular field configurations support the propagation of such modes which are able to spread into a large volume (see Fig. 17). Nevertheless, the vast majority of these motions are still subsonic (see Fig. 18).

Based on our presented study we conclude that collimated jets from young stellar objects are unlikely drivers of large-scale *supersonic* turbulence in molecular clouds. Alternatively it could be powered by large scale flows which might be responsible for the formation of the cloud itself (e.g., Ballesteros-Paredes et al. 1999). Energy cascading down from the driving scale to the dissipation scale will then produce turbulent density and velocity structure in the inertial range in between (Lesieur 1997). If the large-scale dynamics of the interstellar medium is driven by gravity (as suggested, e.g., by Li et al. 2005; Li et al. 2006) gravitational contraction would also determine to a large extent the internal velocity structure of the cloud. Otherwise, blast waves and expanding shells from super novae are also viable candidates to power supersonic turbulence in molecular clouds(see e.g., Mac Low & Klessen 2004).

We thank Mordecai Mac Low for his valuable comments on this work. The FLASH code was developed in part by the DOE-supported Alliances Center for Astrophysical Thermonuclear Flashes (ASC) at the University of Chicago. RB is funded by the Deutsche Forschungsgemeinschaft (DFG) under the grant no. KL1358/4-1.

REFERENCES

- Anderson, J. M., Li, Z.-Y., Krasnopolsky, R., & Blandford, R. D. 2003, ApJ, 590, L107
- Andre, P., Ward-Thompson, D., & Barsony, M. 2000, Protostars and Planets IV, 59
- Bacciotti, F., Ray, T. P., Mundt, R., Eisloffel, J., & Solf, J. 2002, ApJ, 576, 222

- Ballesteros-Paredes, J., Hartmann, L., & Vázquez-Semadeni, E. 1999, *ApJ*, 527, 285
- Ballesteros-Paredes, J., Klessen, R. S., Mac Low, M.-M., & Vázquez-Semadeni, E. 2007, in *Protostars and Planets V*, ed. B. Reipurth, D. Jewitt, & K. Keil, 63–80
- Blandford, R. D., & Payne, D. G. 1982, *MNRAS*, 199, 883
- Chernin, L., Masson, C., Gouveia dal Pino, E. M., & Benz, W. 1994, *ApJ*, 426, 204
- Crutcher, R. M., Troland, T. H., Lazareff, B., Paubert, G., & Kazès, I. 1999, *ApJ*, 514, L121
- Cunningham, A. J., Frank, A., & Blackman, E. G. 2006a, *ApJ*, 646, 1059
- Cunningham, A. J., Frank, A., Quillen, A. C., & Blackman, E. G. 2006b, *ApJ*, 653, 416
- de Gouveia Dal Pino, E. M. 1999, *ApJ*, 526, 862
- Downes, T. P., & Cabrit, S. 2003, *A&A*, 403, 135
- Downes, T. P., & Ray, T. P. 1999, *A&A*, 345, 977
- Elmegreen, B. G., & Scalo, J. 2004, *ARA&A*, 42, 211
- Falgarone, E., Lis, D. C., Phillips, T. G., Pouquet, A., Porter, D. H., & Woodward, P. R. 1994, *ApJ*, 436, 728
- Fendt, C. 2006, *ApJ*, 651, 272
- Fendt, C., & Čemeljić, M. 2002, *A&A*, 395, 1045
- Fryxell, B., Olson, K., Ricker, P., Timmes, F. X., Zingale, M., Lamb, D. Q., MacNeice, P., Rosner, R., Truran, J. W., & Tufo, H. 2000, *ApJS*, 131, 273
- Gueth, F., & Guilloteau, S. 1999, *A&A*, 343, 571
- Heitsch, F., & Burkert, A. 2002, in *Astronomical Society of the Pacific Conference Series*, Vol. 285, *Modes of Star Formation and the Origin of Field Populations*, ed. E. K. Grebel & W. Brandner, 13–+
- Henney, W. J. 1995, in *Revista Mexicana de Astronomia y Astrofisica Conference Series*, ed. M. Pena & S. Kurtz, 89–+
- Hillenbrand, L. A. 1997, *AJ*, 113, 1733
- Klessen, R. S. 2000, *ApJ*, 535, 869
- Klessen, R. S. 2003, in *Reviews in Modern Astronomy*, Vol. 16, *Reviews in Modern Astronomy*, ed. R. E. Schielicke, 23–+

- Knee, L. B. G., & Sandell, G. 2000, *A&A*, 361, 671
- Li, Y., Mac Low, M.-M., & Klessen, R. S. 2005, *ApJ*, 626, 823
- Lada, C. J., & Fich, M. 1996, *ApJ*, 459, 638
- Lesieur, M. 1997, *Turbulence in Fluids* (Kluwer Academic Publishers, Dordrecht)
- Li, Y., Klessen, R. S., & Mac Low, M.-M. 2003, *ApJ*, 592, 975
- Li, Y., Mac Low, M.-M., & Klessen, R. S. 2006, *ApJ*, 639, 879
- Li, Z.-Y., & Nakamura, F. 2006, *ApJ*, 640, L187
- Lis, D. C., Pety, J., Phillips, T. G., & Falgarone, E. 1996, *ApJ*, 463, 623
- Mac Low, M.-M. 1999, *ApJ*, 524, 169
- Mac Low, M.-M. 2000, in *ESA SP-445: Star Formation from the Small to the Large Scale*, ed. F. Favata, A. Kaas, & A. Wilson, 457–+
- Mac Low, M.-M., Balsara, D. S., Kim, J., & de Avillez, M. A. 2005, *ApJ*, 626, 864
- Mac Low, M.-M., & Klessen, R. S. 2004, *Reviews of Modern Physics*, 76, 125
- Mac Low, M.-M., Klessen, R. S., Burkert, A., & Smith, M. D. 1998, *Physical Review Letters*, 80, 2754
- Matzner, C. D. 2007, e-print: astro-ph/0701022, accepted by *ApJ*
- Micono, M., Bodo, G., Massaglia, S., Rossi, P., & Ferrari, A. 2000, *A&A*, 364, 318
- Moraghan, A., Smith, M. D., & Rosen, A. 2006, *MNRAS*, 371, 1448
- Mundt, R., Buehrke, T., Solf, J., Ray, T. P., & Raga, A. C. 1990, *A&A*, 232, 37
- Norman, C., & Silk, J. 1980, *ApJ*, 238, 158
- Ossenkopf, V., & Mac Low, M.-M. 2002, *A&A*, 390, 307
- O’Sullivan, S., & Ray, T. P. 2000, *A&A*, 363, 355
- Ouyed, R., & Pudritz, R. E. 1997, *ApJ*, 482, 712
- Padoan, P., Bally, J., Billawala, Y., Juvela, M., & Nordlund, Å. 1999, *ApJ*, 525, 318
- Padoan, P., Nordlund, Å., Kritsuk, A. G., Norman, M. L., & Li, P. S. 2007, *ApJ*, 661, 972
- Pudritz, R. E., & Norman, C. A. 1983, *ApJ*, 274, 677

- Pudritz, R. E., Ouyed, R., Fendt, C., & Brandenburg, A. 2007, in *Protostars and Planets V*, ed. B. Reipurth, D. Jewitt, & K. Keil, 277–294
- Quillen, A. C., Thorndike, S. L., Cunningham, A., Frank, A., Gutermuth, R. A., Blackman, E. G., Pipher, J. L., & Ridge, N. 2005, *ApJ*, 632, 941
- Raga, A., Cabrit, S., Dougados, C., & Lavalley, C. 2001, *A&A*, 367, 959
- Raga, A. C., & Canto, J. 1995, in *Revista Mexicana de Astronomia y Astrofisica Conference Series*, ed. M. Pena & S. Kurtz, 47–+
- Ray, T., Dougados, C., Bacciotti, F., Eisloffel, J., & Chrysostomou, A. 2007, in *Protostars and Planets V*, ed. B. Reipurth, D. Jewitt, & K. Keil, 231–244
- Reipurth, B., & Bally, J. 2001, *ARA&A*, 39, 403
- Rosen, A., & Smith, M. D. 2004, *A&A*, 413, 593
- Smith, M. D., Mac Low, M.-M., & Heitsch, F. 2000, *A&A*, 362, 333
- Stahler, S. W. 1994, *ApJ*, 422, 616
- Stanke, T. 2000, PhD thesis, , Univ. Potsdam, (2000)
- Stanke, T., McCaughrean, M. J., & Zinnecker, H. 2002, *A&A*, 392, 239
- Stone, J. M., Ostriker, E. C., & Gammie, C. F. 1998, *ApJ*, 508, L99
- Vazquez-Semadeni, E. 1994, *ApJ*, 423, 681
- Warin, S., Castets, A., Langer, W. D., Wilson, R. W., & Pagani, L. 1996, *A&A*, 306, 935